Biosensors and Bioelectronics 195 (2022) 113668

Contents lists available at ScienceDirect

Biosensors and Bioelectronics

journal homepage: www.elsevier.com/locate/bios

Clinical application of serological Alzheimer's disease diagnosis using a highly sensitive biosensor with hydrogel-enhanced dielectrophoretic force

Hye Jin Kim [a,1], Woongsun Choi [b,c,1], Jin San Lee [d], Jungkyu Choi [c,*], Nakwon Choi [b,e,f,**], Kyo Seon Hwang [a,***]

[a] Department of Clinical Pharmacology and Therapeutics, College of Medicine, Kyung Hee University, Seoul 02447, Republic of Korea
[b] Brain Science Institute, Korea Institute of Science and Technology (KIST), Seoul, 02792, Republic of Korea
[c] Department of Chemical and Biological Engineering, Korea University, Seoul, 02841, Republic of Korea
[d] Department of Neurology, Kyung Hee University Hospital, College of Medicine, Kyung Hee University, Seoul 02447, Republic of Korea
[e] KU-KIST Graduate School of Converging Science and Technology, Korea University, Seoul 02841, South Korea
[f] Division of Bio-Medical Science & Technology, KIST School, Korea University of Science and Technology (UST), Seoul, 02792, Republic of Korea

ARTICLE INFO

Keywords:
Porosity-tunable hydrogel
Hopping dielectrophoretic force
Amyloid-beta
Plasma-based diagnosis
Alzheimer's disease

ABSTRACT

Analysis of a ratio between amyloid beta 1–40 and 1–42 ($A\beta_{1\text{-}40}$ and $A\beta_{1\text{-}42}$) presented in plasm enables a highly accurate diagnosis of Alzheimer's disease (AD). However, the analysis of plasma Aβs is not routinely conducted because of the lack of Aβ detection techniques sensitive enough to specifically detect Aβ from thousands of biomaterials present in the plasma. We developed a hydrogel-patterned spiral microelectrode sensor combined with a hopping dielectrophoretic (DEP) force, combining the negative DEP and positive DEP forces, for Aβ detection. The hydrogel effectively increased the number of immobilized fragmented antibodies in the reaction region of the sensor and enabled size-exclusive passive filtration of non-specific plasma proteins from that region. The hopping DEP force further concentrated the Aβs and removed the non-specific plasma proteins. Consequently, our sensor achieved a limit of detection (LOD) of approximately ~ 0.15 pg/mL for both $A\beta_{1\text{-}40}$ and $A\beta_{1\text{-}42}$ in the standard plasma. Finally, comparing the ratio between $A\beta_{1\text{-}40}$ and $A\beta_{1\text{-}42}$ signals, we distinguished AD patients from cognitively normal subjects with 95.83% accuracy and 92.31% precision ($n = 24$, $p < 0.0001$, One-way ANOVA).

1. Introduction

Alzheimer's disease (AD) is a representative type of neurodegenerative disorder that causes severe deterioration in thinking, learning, and organizational abilities and irreversible memory loss (Wong, 2020). And many countries worldwide rapidly turn into aging societies, the number of AD patients continuously increases, and consequently, the direct and indirect socio-economic costs of AD are projected to reach approximately $1 trillion by 2050 (Wong, 2020). For this reason, early diagnosis of AD has been persistently recognized as a very significant global social and economic issue, and various efforts are being made to develop technologies for the early diagnosis of AD. Nevertheless, currently commercialized early diagnostic techniques for AD are limited to cognitive function tests such as mini-mental state examination (MMSE) and neuroimaging (such as positron emission tomography (PET) and magnetic resonance image (MRI)) (Arevalo-Rodriguez et al., 2013; Dos Santos Picanco et al., 2018) which have low accuracy, and high radiation exposure and cost burden, respectively (Citron, 2002; Saint-Aubert et al., 2013; Lin, 2010). Recently, methods of diagnosing AD by detecting Aβ in various physiological body fluids are emerging as a solution to overcome the limitations of existing methods (Balasa et al., 2020; Khoury and Ghossoub, 2019). In particular, Aβ presented in the plasma, announced in 2018 by the National Institute on Aging and Alzheimer's Association (NIA-AA) (J. C. Lee et al., 2019), is attracting attention due to its high correlation with the concentration of Aβ accumulated in the brain and less-invasive sampling process.

* Corresponding author. Department of Chemical and Biological Engineering, Korea University, Seoul, 02841, Republic of Korea.
** Corresponding author. Brain Science Institute, Korea Institute of Science and Technology (KIST), Seoul, 02792, Republic of Korea.
*** Corresponding author. Department of Clinical Pharmacology and Therapeutics, College of Medicine, Kyung Hee University, Seoul 02447, Republic of Korea.
E-mail addresses: jungkyu_choi@korea.ac.kr (J. Choi), nakwon.choi@kist.re.kr (N. Choi), k.hwang@khu.ac.kr (K.S. Hwang).
[1] These authors contributed equally to this study.

https://doi.org/10.1016/j.bios.2021.113668
Received 20 July 2021; Received in revised form 21 September 2021; Accepted 22 September 2021
Available online 24 September 2021

Furthermore, it has also been demonstrated that diagnosing AD with a ratio of $A\beta_{1\text{-}40}$ and $A\beta_{1\text{-}42}$ composed of amino acids of different lengths increases diagnostic accuracy (Fandos et al., 2017; Hansson et al., 2019). However, studies on AD diagnosis by detecting Aβs in plasma have been restrictively executed so far due to the low sensitivity of the sensor in plasma. The low sensitivity of the sensor in plasma is caused by the non-specific adsorption of various plasma proteins, and is directly related to the diagnostic accuracy and reliability, so increasing the sensor's sensitivity is a very significant issue for plasma-based AD diagnosis.

In our previous studies, we used two approaches to implement highly sensitive biosensors (Kim et al., 2016, 2019, 2020). The first approach was to control the location of various biomolecules, including the target molecules, in plasma with a dielectrophoretic (DEP) force generated in a inhomogeneous electric field (***E***-field) (Kim et al., 2019). The DEP force, whose strength and direction are controlled according to the size of molecules and the intensity and frequency of the applied voltage, is generated within the region where the ***E***-field is formed, providing high accessibility and convenience (Abd Rahman et al., 2017). Using the DEP force, we generated an active filtration effect in the reaction region of the biosensor to selectively concentrate the target and remove the non-specific biomaterials, resulting in a highly sensitive Aβ analyses. Meanwhile, in the second method, a highly sensitive biosensor was implemented using a porous hydrogel at the reaction region (Kim et al., 2020). The Poly (ethylene glycol) (PEG)-based hydrogel consists of more than 90% of water and a three-dimensional (3D) mesh structure with excellent biocompatibility (Naahidi et al., 2017). Additionally, PEG-based hydrogels show a high antifouling property due to the neutral charge and absence of the hydrogen bond donors (Ekblad et al., 2008; Murosaki et al., 2011; Ostuni et al., 2001). Moreover, one can easily incorporate various biologically recognizable receptors such as DNA oligomers and antibodies for specific detection of desired targets (Le Goff et al., 2015; Buenger et al., 2012). Due to favorable properties of hydrogels, many researchers have utilized hydrogel-based sensors in clinical trials such as implantable glucose sensors (Sawayama et al., 2021; Tokuda et al., 2014) virus-detectable sensors (Kim et al., 2018; Wang and Li, 2013). Based on the hydrogel properties, we spatially immobilized the antibody inside the hydrogel pattern while increasing the antigen-antibody binding probability by utilizing the size-exclusive passive filtration effect that occurs through the size control of the hydrogel's pore, demonstrating a high sensitivity of Aβ analysis. These previous studies suggested that the immobilization of the antibody and the selective filtration effect of target and non-specific substances would enable more sensitive plasma-based the Aβ analysis.

Here, we demonstrate the feasibility of plasma-based AD diagnosis with high accuracy by simultaneously utilizing the synergistic effects of hydrogel and DEP force to implement a biosensor to maximize sensitivity (Fig. 1). Our sensor was based on an optimal spiral microelectrodes (SMEs) structure covered with a hydrogel with an optimized pore size and thickness, in which fragmented antibodies were immobilized in the hydrogel surface. The hydrogel improved the density of immobilized antibodies, and enabled a passive filtration effect that prevents non-specific adsorption. Furthermore, we generated an active filtration effect in the SMEs sensor by applying the DEP force to maximize the sensor's sensitivity. As a result, the sensitivity in the Aβ analysis was improved up to approximately 2.227 times compared to the value of the bare SMEs sensor without hydrogel patterns and DEP force. Finally, we quantified the ratio between $A\beta_{1\text{-}40}$ and $A\beta_{1\text{-}42}$ in the plasma of AD patients and demonstrated excellent AD diagnostic performance with 95.83% accuracy and 92.31% precision ($n = 24$, $p < 0.0001$, one-way ANOVA).

2. Material and methods

2.1. Reagents and materials

All materials are listed in the online supplemental material (Supporting **Note 1**).

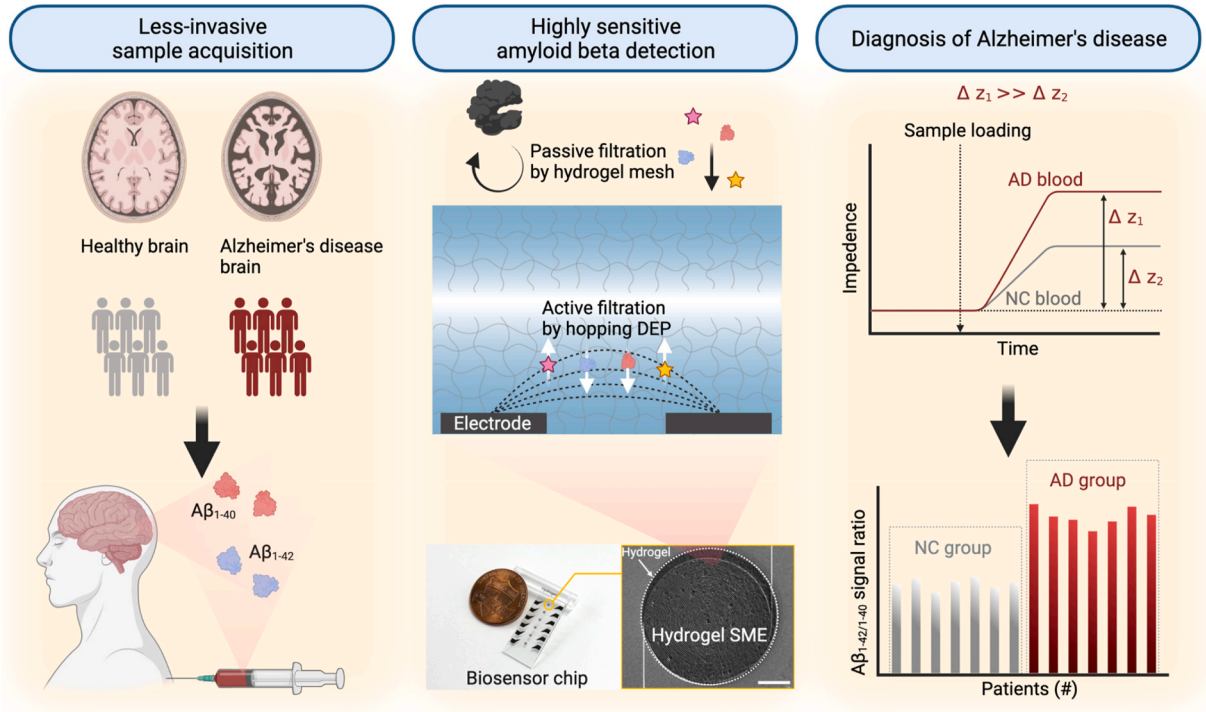

Fig. 1. Schematic illustration of a hydrogel-embedded highly sensitive biosensor driven by dielectrophoretic (DEP) force. Figure created using BioRender (https://bioRender.com/).

2.2. Fabrication of the sensor, surface functionalization and sensor's signal processing

A single biosensor chip with a width and length of 10 mm and 24 mm, respectively, consisted of six single spiral SME sensors fabricated through a standard micro electro mechanical system (MEMS) process (Figs. S1a–b). Further details were described in Supporting **Note 2**.

2.3. Optimization of the thickness and pore size of the hydrogels

With three different hydrogel prepolymers, hydrogel-based microposts were fabricated to optimize the pore sizes of the hydrogel matrices. For the 20% PEG700DA prepolymer, 20% [v/v] PEG700DA, 40% [v/v] PEG600, 35% [v/v] 30 mM PBS, and 5% [v/v] photoinitiator were mixed. For the 30% PEG700DA prepolymer, 30% [v/v] PEG700DA, 30% [v/v] PEG600, 35% [v/v] 30 mM PBS, and 5% [v/v] photoinitiator were mixed. For the 40% PEG700DA prepolymer, 40% [v/v] PEG700DA, 20% [v/v] PEG600, 35% [v/v] 30 mM PBS, and 5% [v/v] photo-initiator were mixed. A droplet of the prepolymer was loaded on the surface of 24 × 60 mm slide glasses, and 22 × 22 mm cover glasses were covered with a double-sided tape (150 μm thickness) as a spacer. The prepolymer was placed on an inverted microscope (Axio Observer A1, Carl Zeiss, Germany) and exposed to collimated ultraviolet (UV, wavelength: 365 nm) light at 80 mJ/cm^2 through a circular (diameter: 1800 μm) film photomask. The fabricated hydrogel microposts were rinsed with flowing DW, and the filled water between the two glasses was wiped. To adjust the optimal thickness of the hydrogel structure, 30% PEG700DA prepolymer was mixed with methacryloxyethyl thiocarbamoyl rhodamine B in a volume ratio of 9:1 and spin-coated (spin-1200D, MIDAS Systems, Korea) on a glass substrate at various rpms. Then, the hydrogel-coated glass was exposed to UV light as described above. Hydrogel structures were imaged with a 20× magnification lens on a confocal microscope (LSM700, Carl Zeiss, Germany). Z-stacked images (step size, 1 μm) were acquired to determine the height of the hydrogel structures. The pore size of the hydrogels was analyzed by measuring the fluorescence intensity of the hydrogel microposts using an sCMOS camera (OptiMOS, QImaging, exposure time: 100 ms) and Image J (NIH).

2.4. Patterning of the hydrogel on the sensors and antibody immobilization

The hydrogel was patterned on the surface of the spiral IME sensor through a chemical functionalization process. The sensor surface was cleaned with piranha solution, DW, and EtOH to remove organic and inorganic residues. Subsequently, the surface was subjected to O_2 plasma treatment (power: 100 W, for 5 min) and then treated with TMSPMA (50 wt% (w/v) in EtOH) and BP (5 mg/mL in acetone) at 37 °C for 1 h, followed by washing with acetone and DW. The BP was photochemically activated by exposing the sensor surface to UV light for 15 s (total energy: 60 mW) in a UV chamber (MT-GJ60, MINUTA Technology, Osan-si, Korea) to enhance the adhesion between the sensor surface and the hydrogel pattern (Leigh et al., 2018; Schneider et al., 2011). After BP activation, the hydrogel prepolymers were evenly coated on the sensor surface using a spin-coater (spin-1200D, MIDAS Systems, Korea) and patterned using the same methods and conditions described in Section 2.3. Finally, the fragmented antibody was three-dimensionally immobilized on the hydrogel pattern at 37 °C for 48 h, followed by washing with 1 mM PBS to remove the unbound antibodies.

2.5. Plasma acquisition and sampling protocol

Written informed consent was obtained from all the participants prior to inclusion in the study. The study was approved by the Institutional Review Board (IRB) of Kyung Hee University Hospital (IRB#. 2018-01-023). The details were described in Supporting **Note 3**.

3. Results

3.1. Fabrication of spiral microelectrode (SMEs) sensor

The performance of the hydrogel-patterned SME sensor was affected by 1) the geometry of the sensor, 2) structural properties of the hydrogel, such as thickness and pore size, and 3) the density of the immobilized antibody. Therefore, the sensitivity of the bare SME sensor was first verified according to various widths, intervals, and electrode numbers to optimize the geometry of the sensor. The width and interval between the SMEs and the number of electrode pairs were designed (Fig. S1c), considering the diameter of the passivation holes. Thereafter, $A\beta_{1\text{-}42}$ specific antibody was immobilized on the surface of the bare SME sensor (Supplementary material, Note 1), and 100 pg/mL $A\beta_{1\text{-}42}$ in 0.1 mM PBS was analyzed. As a result, as the width and interval and the number of SMEs increased, the sensitivity of the SME sensor increased, and the manufacturing yield decreased (Figs. S1d–e). The manufacturing yields were approximately 81.25% and 72.92% when the number of SMEs was 10 and 20 pairs, respectively, in the sensor composed of 5 μm wide and spaced SMEs, while the yield was less than 65% for the sensors with 10 pairs of SMEs with a 3 μm width and spacing. In particular, the manufacturing yield of 20 pairs of bare SME sensors with a width and spacing of 3 μm was extremely poor (approximately 33%). Thus, we confirmed the sensitivity of three SME sensors for $A\beta_{1\text{-}42}$ detection, and the sensitivities were approximately 0.236, 0.110, and 0.238 for the sensor consisting of 10 pairs of SME sensors with a 5 μm width and interval and a 3 μm width and interval and 20 pairs of SMEs with a 5 μm width and interval, respectively. Based on the results, the width and interval and the number of SMEs were fixed at 5 μm and 20, respectively.

3.2. Optimizing the structural properties of hydrogel patterns

We improved the performance of the SME sensor by optimizing the structure of the hydrogel pattern formed on the surface of the SME sensor and immobilizing fragmented antibodies to induce alignment inside the patterns (Fig. 2a). To induce a size-exclusive filtration effect that blocks unwanted components, the pore size of the hydrogel was designed to be slightly larger than the size of the target molecules by changing the composition of PEG700DA from 20% to 40% [v/v]. The pore size was confirmed by measuring the partition coefficient (K) of FITC-dextran 10 kDa and 150 kDa with hydrodynamic diameters of 4.6 and 17 nm, respectively, within the hydrogel microposts. The partition coefficient represents the ratio of the diffused FITC-dextran from the exterior to the interior of the hydrogel. The results confirmed that the average radius of the effective pore size was smaller than 4.6 nm in the hydrogel photocrosslinked with 40% PEG700DA (Fig. 2b). By contrast, in the hydrogel with 20% PEG700DA, both 10 kDa and 150 kDa dextran diffused into the hydrogel, indicating that the pore size of the hydrogel was larger than 17 nm, indicating a lack of filtration effect. Thus, a 30% proportion of PEG700DA was selected to allow target molecules to diffuse into the hydrogel without significant hindrances and large molecules to be filtered out.

Meanwhile, the height of the hydrogel patterned on the surface of the SME sensor was determined by comparing the sensitivity and fabrication yield depending on the thickness of the hydrogel pattern. The height of the hydrogel was approximately 33.5, 30, and 28 μm at 1000 rpm, 2000 rpm, and 3000 rpm, respectively (Fig. 2c; Fig. S2). The hydrogel patterning yields on the SME sensor were changed according to the height of the hydrogel. The patterning yield of the 33.5 μm hydrogel patterns was approximately 87.72%, but as the thickness was decreased, the yield decreased to approximately 55.56% and 30.56%, and no pattern was formed at lower pattern heights (Fig. 2d). However, hydrogel height showed little correlation with the sensor's sensitivity of the sensor, although the sensitivity of the hydrogel-patterned SME

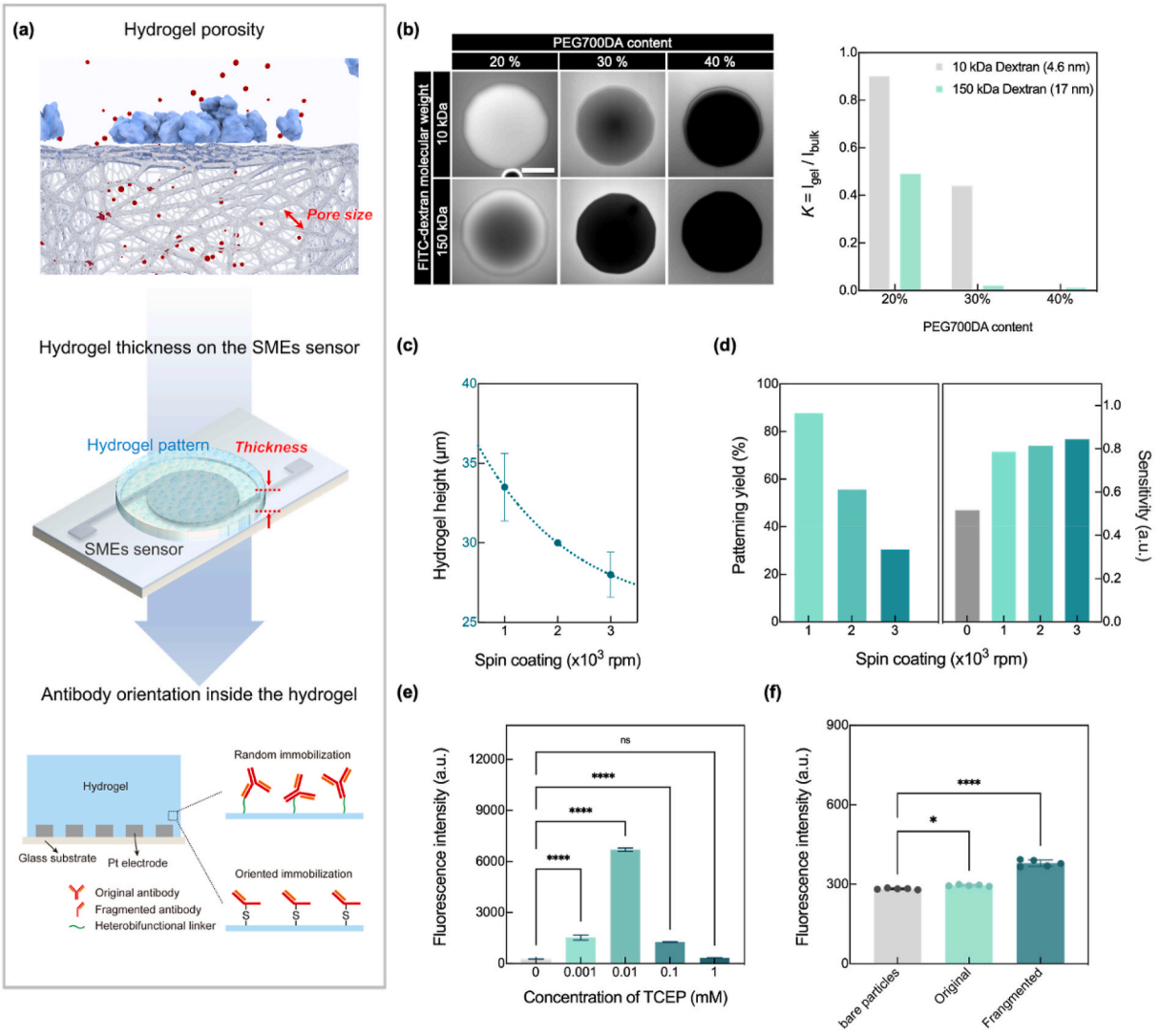

Fig. 2. **(a)** Optimization process of the structural properties of hydrogel pattern. **(b)** Fluorescence intensity of hydrogel microposts with various pore sizes. Scale bar = 50 μm. **(c)** Height of the hydrogel patterns according to the spin coating rpm of the hydrogel. **(d)** Patterning yield and sensitivity of the hydrogel-patterned SME sensor in various hydrogel patterning conditions. **(e)** Fluorescence intensity of hydrogel microposts immobilized with fluorescence-labeled antibodies, following treatment with antibody reduction conditions. **(f)** Comparing the fluorescence intensity in the microposts immobilized with the fluorescence-labeled antibodies. The 'Original' and 'Fragmented' refer to the antibodies that have not undergone or undergone reduction, respectively. ****$p < 0.0001$; ***$p < 0.001$; **$p < 0.01$; *$p < 0.05$, One-way ANOVA. Data in **(c)**, **(e)**, and **(f)** are mean ± SD.

sensor increased approximately 1.528-fold compared with that of the bare SME sensor without the hydrogel pattern. The sensitivity of the bare SME sensor was approximately 0.516, and for the hydrogel-patterned SME sensor, it was 0.788, 0.814, and 0.84, depending on the coating speed. Such a low correlation between the thickness of the hydrogel pattern and the sensitivity of the sensor occurred because even the lowest thickness of the hydrogel pattern (spin coating speed = 3000 rpm) was sufficiently higher than 10 μm, the height at which 95% of the ***E***-field was formed between the electrodes (Fig. S3) (Van Gerwen et al., 1998). Therefore, the thickness of the hydrogel was fixed at 33.5 μm, as it showed the highest patterning yield.

3.3. *Immobilization of the fragmented antibodies inside the hydrogel*

We adopted the thiol-ene reaction between residual double bonds in the hydrogel and free thiols in the fragmented antibody to immobilize the antibodies inside the hydrogel. After patterning the hydrogel, unreacted double bonds remain, which are not activated by free-radicals (Le Goff et al., 2015; Pregibon and Doyle, 2009). Additionally, fragmented antibodies reduced with TCEP possess free thiols (Alonso et al., 2018; Makaraviciute et al., 2016) (The detail process is described in Supporting **Note 4**). When a low concentration of TCEP was used, TCEP was not sufficient to reduce the disulfide bonds to generate free thiols in the antibody. Contrastingly, high concentrations of TCEP reduce all disulfide bonds in an antibody, resulting in dysfunction of the antibody (H. J. Lee et al., 2019). To optimize the TCEP concentration in the antibody fragmentation step, we fabricated microposts and attached FAM-tagged antibodies fragmented with different TCEP concentrations (Fig. 2e; Fig. S4). The fluorescence intensity of hydrogel microposts showed the highest incorporation of antibodies at 0.01 mM TCEP. These data indicate that antibodies were excessively fragmented above and not reduced below 0.01 mM TCEP. Hence, we chose 0.01 mM TCEP as the optimal concentration for the effective incorporation of antibodies. The orientation of immobilized antibodies is significant because it affects the accessibility of antigens to the paratope of antibodies (Kausaite-Minkstimiene et al., 2010). The most widely used method for immobilization of antibodies is the use of amine-reactive crosslinkers. These linkers bind to the primary amines in antibodies, and the functional groups in the

linkers can connect the antibody linker to the desired surface. However, this often leads to poor performance of a biosensor because of its random orientation. Alternatively, fragmented antibodies are well-oriented because the location of free thiols is controllable under adequate conditions. First, we compared the incorporation efficiency of the original antibodies with the heterobifunctional linker (randomly oriented) and fragmented antibodies (well-oriented) in the hydrogel with FAM-tagged antibodies. With the same concentration of antibodies, the fragmented antibodies showed 7.5 times increase in fluorescence intensity compared to that of the original antibodies with the subtracted fluorescence intensity of bare hydrogels. Therefore, the immobilization using the free thiols of fragmented antibodies was more efficient than

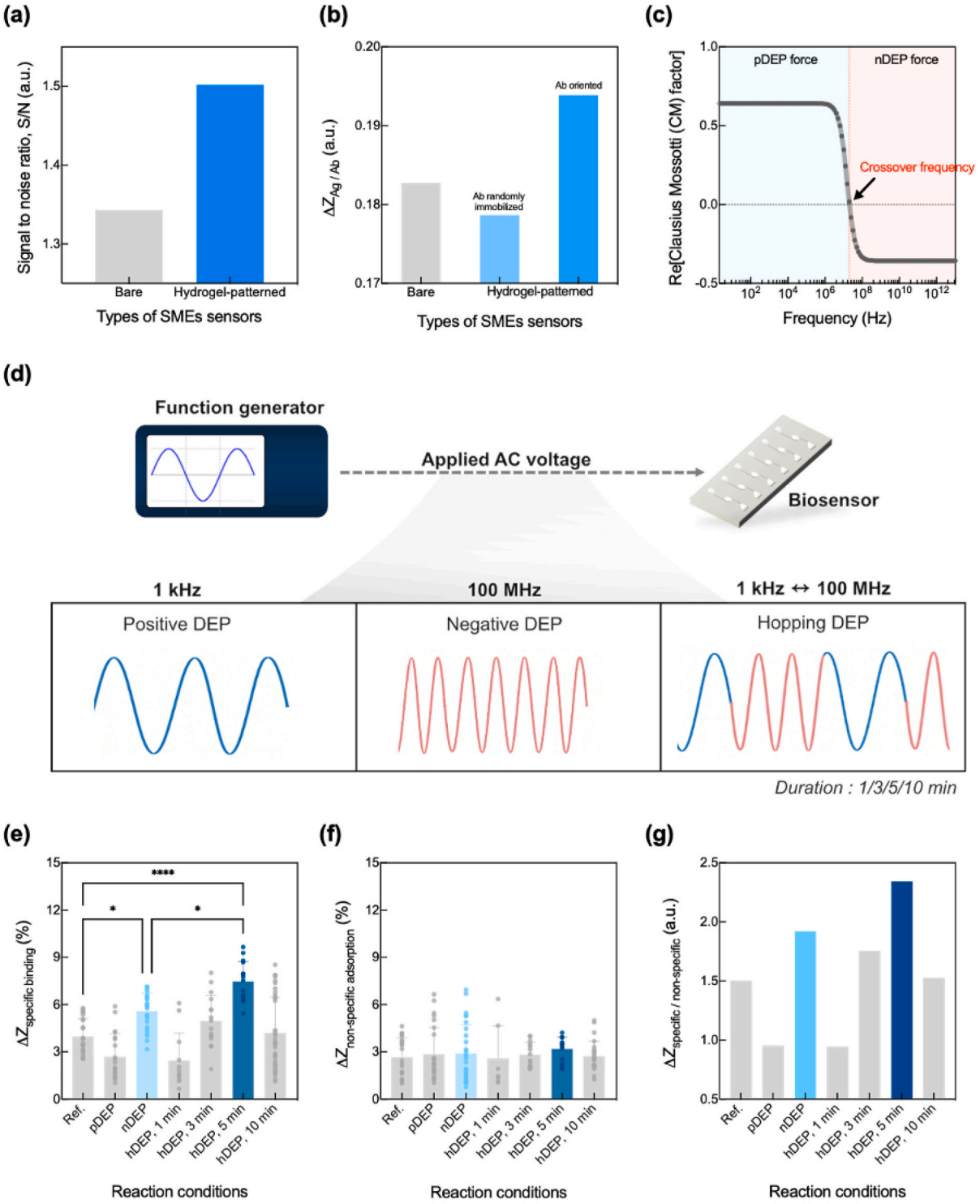

Fig. 3. Enhancing the performance of the hydrogel-patterned SME sensor using DEP force. **(a)** Signal to noise ratio (S/N) in the bare and hydrogel-patterned SME sensors. **(b)** Comparing the signals by antibody immobilization ($\Delta Signal_{Ab}$) and antigen reaction ($\Delta Signal_{Ag}$) in the bare SME sensor and hydrogel-patterned SME sensors in which antibody was randomly or uniformly immobilized. **(c)** Verifying the crossover frequency of the DEP force. **(d)** Illustration of the positive, negative, and hopping DEP forces. The impedance changes of the hydrogel-patterned SME sensor by **(e)** specific binding of $A\beta_{1\text{-}42}$ and **(f)** non-specific adsorption of Tau in various DEP conditions. **(g)** Ratio between the specific and non-specific signals in various DEP conditions.

using the amine-reactive linker conjugated to the original antibodies.

3.4. Maximizing the performance of hydrogel-patterned SME sensor by hopping DEP

The hydrogel-patterned SMEs sensor showed a high stability (Supporting **Note 5**). Also, our sensor showed a higher impedance change in the detection of 100 pg/mL $A\beta_{1\text{-}42}$ than the impedance change in the bare SME sensor, whereas the changes due to non-specific adsorption of 10 pg/mL tau were not significantly different between the two types of sensors (Fig. S5). The impedance change was approximately 2.824 ± 0.345% in the bare SME sensor and was improved approximately 1.411-folds by the optimized hydrogel patterning (3.985 ± 1.091%, $p < 0.01$, one-way ANOVA), and the changes due to non-specific adsorption of 10 pg/mL tau in 0.1 mM PBS were measured to be approximately 2.104 ± 0.738% and 2.653 ± 1.214% in bare and hydrogel-patterned SME sensors, respectively. Based on the impedance changes, the signal-to-noise ratio (S/N) was calculated by dividing the signal of the specific binding by that of non-specific adsorption, and it was demonstrated that the S/N was higher in the hydrogel-patterned SME sensor than in the bare SME sensor (Fig. 3a). The S/N values of the bare and hydrogel-patterned SME sensors were approximately 1.343 and 1.502, respectively. Moreover, it was demonstrated that immobilization of the oriented antibody increased the binding affinity of the antibody-antigen and the density of the antibody immobilized inside the hydrogel (Fig. 3b). The antibody-antigen binding affinity was verified by dividing the impedance changes due to the antigen reaction by the changes caused by antibody immobilization, and the changes by antibody immobilization and antigen reaction were approximately 15.46 ± 1.119%, 18.86 ± 1.929%, and 21.00 ± 3.431% and approximately 2.824 ± 0.173, 3.369 ± 0.376, and 4.072 ± 0.537 in the bare and hydrogel-patterned SME sensors, where the antibody was immobilized randomly or in an oriented manner, respectively (Fig. S6). Consequently, for the three types of SME sensors, the ratios between the antibody and antigen signals were approximately 0.183, 0.179, and 0.194, respectively.

The DEP force arising from a non-uniform ***E***-field can focus the target molecules in a specific region depending on the frequency and strength of the applied alternating current (AC) voltage (Supporting **Note 6**). The type of DEP force is determined based on the Clausius-Mossotti (CM) factor, which ranges from −1 to 1 depending on the frequency of the applied AC voltage (Kim et al., 2016). When the CM factor is less than zero (i.e., the value of the CM factor is negative), a negative DEP (nDEP) force is induced in the ***E***-field region, causing the molecules to move away from the dense ***E***-field region (Kim et al., 2016). However, if the CM factor is greater than zero (i.e., the value of the CM factor is positive), a positive DEP (pDEP) force, which attracts the molecules to the dense ***E***-field region, is generated. In general, other groups have individually utilized nDEP or pDEP forces to manipulate molecules; however, here, we combined nDEP and pDEP forces to simultaneously attract and push the molecules in the reaction region of the sensor. The force combining the nDEP and pDEP forces, namely, the hopping DEP (hDEP) force, was generated by applying the nDEP and pDEP forces alternately; consequently, the performance of the hydrogel-patterned SME sensor was further enhanced by the hDEP force. We determined the intensity of voltage to be 0.5 V based on our previous study[14], and optimized the frequency for applying pDEP and nDEP forces by calculating the crossover frequency. The crossover frequency, which is the boundary frequency between the nDEP and the pDEP forces, was confirmed to be approximately 20 MHz through simulation (Fig. 3c); therefore, the frequency conditions for applying pDEP and nDEP were determined to be 1 kHz and 100 MHz, respectively. According to the determined DEP conditions, only the nDEP (or pDEP) force was applied to the hydrogel-patterned SME sensor in the nDEP (or pDEP) condition for 20 min, which was the binding time of 10 pg/mL $A\beta_{1\text{-}42}$ to the immobilized antibody, whereas nDEP and pDEP forces were alternately applied to the sensor in the hDEP condition for 20 min with durations of 1 min, 3 min, 5 min, or 10 min (Fig. 3d). The results demonstrated that, compared to the impedance change of the hydrogel-patterned SME sensor without applying any DEP force ('Ref.'), the pDEP force lowered the impedance change, whereas the nDEP force enhanced this change. The impedance changes were approximately 3.986 ± 1.091%, 2.709 ± 1.420%, and 5.585 ± 1.125% in the Ref., pDEP, and nDEP conditions, respectively ($p < 0.01$ in 'Ref.' vs. nDEP condition, one-way ANOVA). Additionally, a difference in impedance change due to the DEP forces was observed under various hDEP conditions. The impedance change was maximized by up to approximately 7.470 ± 1.213% under the hDEP condition with a duration of 5 min between the nDEP and pDEP forces ($p < 0.0001$ for 'Ref.', one-way ANOVA), but the change decreased under the hDEP condition with durations of 1, 3, and 10 min. By contrast, there were few changes in impedance due to non-specific adsorption under various DEP conditions: the impedance change was approximately 2.653 ± 1.214% in the hydrogel-patterned SME sensor and maximized to approximately 3.189 ± 0.729% in the hydrogel-SME sensor based on the hDEP with a duration of 5 min (Fig. 3f). Consequently, the S/N was enhanced by more than 1.560-times by the hDEP force compared to that of the "Ref" (S/N = 1.502 and 2.342 in the "Ref" and hDEP conditions, respectively), which is superior to the focusing effect using nDEP (S/N = 1.921) (Fig. 3g).

3.5. Highly sensitive analysis of the Aβs in various buffers

The hydrogel-patterned SME sensor enabled the sensitive analysis of $A\beta_{1\text{-}40}$ and $A\beta_{1\text{-}42}$ in 0.1 mM PBS. The average noise level, including system noise and signal changes due to non-specific adsorption of tau, was approximately 1.894%, as indicated by the gray areas in Fig. 4. Depending on the concentration of $A\beta_{1\text{-}40}$, the changes in impedance in the hydrogel-patterned SME sensor were approximately 4.307 ± 0.272%, 5.068 ± 0.690%, 5.815 ± 0.998%, 6.595 ± 0.339%, and 7.039 ± 0.204% in the detection without the hDEP force and 3.980 ± 0.470%, 5.550 ± 0.470%, 6.301 ± 0.561%, 8.500 ± 0.409%, and 9.147 ± 0.251% in the detection with the hDEP force, whereas the changes were approximately 2.763 ± 0.440%, 3.151 ± 0.342%, 3.860 ± 0.264%, 4.433 ± 0.712%, and 5.151 ± 0.198% for the bare SME sensor (Fig. 4a). These results showed that our hydrogel-patterned SME sensor has an excellent limit of detection (LOD; signal-to-noise (SNR) = 3) of 0.15 pg/mL, limit of quantification (LOQ; SNR = 10) of 0.50 pg/mL and a wide dynamic range from 10 fg/mL to 100 pg/mL. We compared the analytical performance of our sensor to previously reported sensors that detected Aβ for diagnosing AD (Table S4). Although the LOD of our sensor is not as low as that of super-sensitive sensors, our sensor fulfilled the clinical needs because it has been demonstrated that $A\beta_{1\text{-}42}$ levels in plasma in patients with AD and controls could be detected from 25 to 85 pg/mL (Mehta et al., 2000). As observed for the $A\beta_{1\text{-}40}$ analysis, the changes in impedance by specific binding of $A\beta_{1\text{-}42}$ in the bare SME sensor were significantly enhanced by patterning the hydrogel on the sensor as well as by applying the hDEP force (Fig. 4b). The changes in the bare SMEs and hydrogel-patterned SME sensors ranged from approximately 2.172 ± 0.112% to 4.101 ± 0.058% and approximately 3.510 ± 0.240% to 6.450 ± 0.903%, depending on the concentration of the $A\beta_{1\text{-}42}$. The changes that occurred in the hydrogel-patterned SMEs with the hDEP force sensor ranged from approximately 3.573 ± 0.281% to 8.049 ± 0.566%, in the various concentration of $A\beta_{1\text{-}42}$. sensitivities were calculated using the linear regression analysis (linear equation: $y = intercept + slope \cdot x$, the value of slope signifies the sensitivity of the sensor for antigen reaction) to quantify the performance improvement of the hydrogel-patterned SME sensor, and the values were up to an average 2.227-fold and 1.695-fold higher in the hydrogel-patterned SMEs with hDEP force, than those measured in other sensors, in the $A\beta_{1\text{-}40}$ and $A\beta_{1\text{-}42}$ analyses, respectively (Fig. 4c). The sensitivities of the bare and hydrogel-patterned SME sensors with and without the hDEP sensor for $A\beta_{1\text{-}40}$ detection were approximately 0.606, 0.699, and 1.329

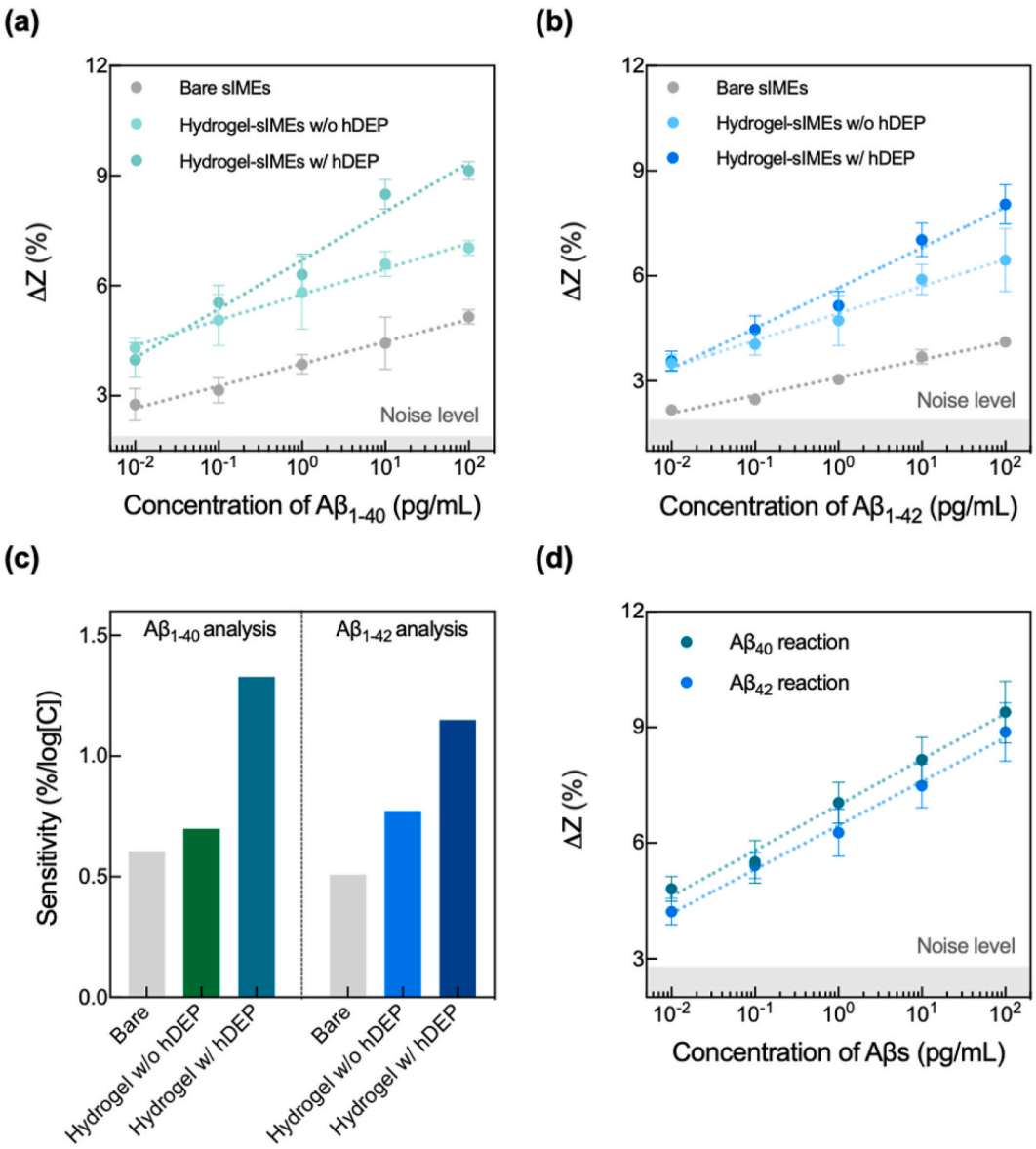

Fig. 4. Basic performance of the hydrogel-patterned SME sensor with hDEP force. Impedance changes of the bare SME sensor and hydrogel-patterned SME sensors without and with hDEP force according to the concentration of **(a)** $A\beta_{1\text{-}40}$ and **(b)** $A\beta_{1\text{-}42}$ in the 0.1 mM PBS. **(c)** Sensitivities in three types of SME sensors. **(d)** Impedance changes of the hydrogel-patterned SMEs with hDEP force according to the concentration of $A\beta_{1\text{-}40}$ and $A\beta_{1\text{-}42}$ in the standard plasma. Dash line in **(a)**, **(b),** and **(d)**: semi log-linear fitting line, $y = y_{intercept} + slope * log(x)$, gray region in **(a)**, **(b),** and **(c)**: noise level. Data in **(a)**, **(b)**, and **(d)** are mean ± SD.

and, for $A\beta_{1\text{-}42}$ analysis, approximately 0.509, 0.773, and 1.150, respectively.

Furthermore, quantitative analysis of $A\beta_{1\text{-}40}$ and $A\beta_{1\text{-}42}$ in the plasma in the presence of various proteins using the hydrogel-patterned SME sensor with hDEP force confirmed that the sensitivity, LOD, and dynamic range of the sensors were similar to those observed in the PBS. The impedance change ranged from approximately 4.814 ± 0.327% to 9.399 ± 0.802% in the $A\beta_{1\text{-}40}$ analysis, and approximately 4.221 ± 0.343% to 8.882 ± 0.764% in the $A\beta_{1\text{-}42}$ analysis (Fig. 4d). From the results, the sensitivities in the $A\beta_{1\text{-}40}$ and $A\beta_{1\text{-}42}$ analyses were calculated to be approximately 1.182 and 1.140, respectively.

3.6. Diagnosis of Alzheimer's disease

Finally, we analyzed the Aβ present in plasma samples extracted from AD subjects, suggesting the high possibility of our hydrogel-patterned SME sensor as a plasma-based early diagnosis platform for AD. The participants were classified into normal controls (NC, $n = 12$) and AD ($n = 12$) subjects based on Aβ-PET positivity, and the average signal levels of $A\beta_{1\text{-}40}$ and $A\beta_{1\text{-}42}$ were significantly different between the two groups (Table 1; Supporting **Note 3**).

As shown in Fig. 5a, most of the impedance changes caused by $A\beta_{1\text{-}40}$ ($A\beta_{1\text{-}40}$ signal) in the NC group were higher than those in the AD group, with average values of approximately 6.349 ± 2.463% and 3.982 ± 1.032%, respectively ($p = 0.006$, one-way ANOVA). By contrast, the average value of impedance changes induced by $A\beta_{1\text{-}42}$ ($A\beta_{1\text{-}42}$ signal) in the AD group was approximately 7.580 ± 1.807%, which was relatively higher than that in the NC group (approximately 5.063 ± 1.744%, $p = 0.003$, one-way ANOVA) (Fig. 5b). Remarkably, the ratio between the $A\beta_{1\text{-}40}$ and $A\beta_{1\text{-}42}$ signals showed dramatically distinctive differences between the NC and AD groups; the average values of $A\beta_{1\text{-}42}/A\beta_{1\text{-}40}$ were approximately 0.882 ± 0.307 and 1.983 ± 0.531 in the AD and NC groups, respectively ($p < 0.0001$, one-way ANOVA) (Fig. 5c). These results are consistent with the hypothesis and previous studies that the level of $A\beta_{1\text{-}42}$ increases, while the level of $A\beta_{1\text{-}40}$ decreases as AD progresses. To evaluate the clinical applicability of our multiplexed

Table 1
Demographics and plasma Aβ analysis of the study participants.

	NC (n = 12)	AD (n = 12)	*p*-value
Gender (M/F)	3/9	4/8	1.000
Age, yr	65.3 (7.3)	72.3 (9.2)	0.049
Education, yr	10.5 (5.1)	7.5 (5.1)	0.160
APOE ε4 status	5 (41.7)	6 (50.0)	0.682
MMSE	26.8 (3.3)	17.0 (4.4)	<0.001
CDR	0.5 (0.0)	0.9 (0.4)	0.005
CDR sum of boxes	0.9 (0.8)	5.9 (3.0)	<0.001
Neuropsychological test			
Attention	−0.3 (0.4)	−1.2 (0.8)	0.003
Language	0.1 (0.9)	−2.4 (2.1)	0.002
Visuospatial	0.6 (0.8)	−4.8 (7.1)	0.025
Memory	−0.5 (0.9)	−2.9 (1.6)	<0.001
Frontal/executive	−0.6 (1.1)	−4.7 (2.8)	<0.001

Values are means (SD) or n (%).
Memory performance was assessed using the Seoul Neuropsychological Screening Battery and presented as a Z-score.
Abbreviations: NC, normal controls; AD, Alzheimer's disease; *APOE*, apolipoprotein E; MMSE, Mini-Mental State Examination; CDR, Clinical Dementia Rating.

biosensing platform for distinguishing AD patients from the NC group, a receiver operating characteristic (ROC) analysis was conducted, and the area under the curve (AUC) of ROC was calculated (Fig. 5d). ROC analysis is a standard statistical method for evaluating the sensitivity, specificity, and accuracy of the sensing platform in disease diagnosis; the value of AUC quantitatively indicates the diagnostic accuracy of a sensing platform. The AUC for the signal of $A\beta_{1\text{-}42}/A\beta_{1\text{-}40}$ was the highest at 0.993, whereas the individual signals of $A\beta_{1\text{-}40}$ and $A\beta_{1\text{-}42}$ showed low AUC values of 0.799 and 0.847, respectively. Additionally, based on the maximum Youden index with a positive percentage agreement of 1.000 (95% CI 0.758–1.000) and a negative percentage agreement of 0.917 (95% CI 0.646–0.996) with Aβ-PET positivity, the participants with $A\beta_{1\text{-}42/1\text{-}40}$ values exceeding 1.273 were considered as AD patients, and the accuracy and precision of AD diagnosis were confirmed to be 95.83% and 92.31%, respectively (Supplementary material, Table S3). Furthermore, the linear regression (*r*) between the Aβ-PET SUVR and plasma $A\beta_{1\text{-}42/1\text{-}40}$ levels was approximately 0.761, indicating high linearity (Fig. 5e). These results demonstrate that the hydrogel-patterned SME sensor with hDEP force can perform plasma-based AD diagnosis with high accuracy and precision.

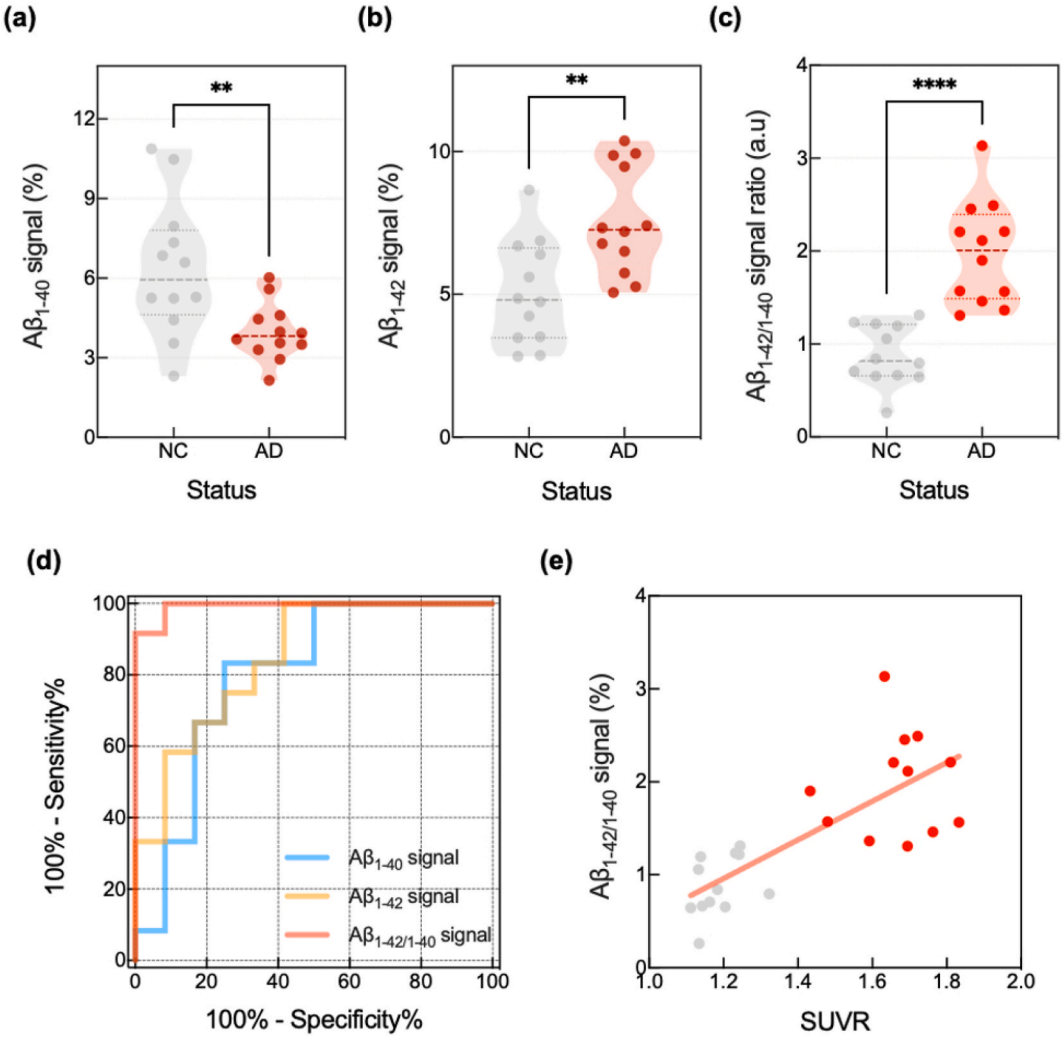

Fig. 5. Diagnosis of AD based on the hydrogel-patterned SME sensor with hDEP force. Distribution of **(a)** $A\beta_{1\text{-}40}$, **(b)** $A\beta_{1\text{-}42}$, and **(c)** $A\beta_{1\text{-}40/1\text{-}42}$ signals from the plasma of AD patients ('AD', n = 12) compared to that of the cognitive normal subjects ('NC', n = 12). **(d)** ROC curve for AD diagnosis based on 12 positive and 12 negative Aβ-PET sera. **(e)** Linear regression of $A\beta_{1\text{-}40/1\text{-}42}$ signals for SUVR. ****$p < 0.0001$; ***$p < 0.001$; **$p < 0.01$; *$p < 0.05$, One-way ANOVA.

4. Discussion

Owing to the properties of the hydrogel (Ahmed, 2015), the S/N of our sensor increased approximately 1.118-fold, and the signal due to the immobilization of the antibody on the reaction region also increased. Furthermore, we maximized the performance of the sensor by additionally applying the DEP effect to the hydrogel-patterned sensor to which the passive filtering effect was applied. In particular, unlike most previous studies, we reproduced dramatic S/N ratio values that were approximately orders of magnitude higher using hDEP forces where pDEP and nDEP forces were periodically applied. As a result, our hydrogel-patterned SME sensor with hDEP force enabled the diagnosis of AD by detecting Aβ, a representative AD biomarker, in real plasma ($n = 24$, $p < 0.0001$, AUC = 0.993). The results showed that our sensor showed high diagnostic accuracy (approximately 95.83%) and precision (approximately 92.31%), as well as a high correlation with SUVR values using amyloid-PET ($r = 0.761$).

The hydrogel-patterned SME sensor we propose is the first biosensor in which structure-based passive and ***E***-field-based active filtration effects are applied simultaneously, and the sensor was fabricated by optimizing not only the dimensions of the sensor but also 1) the structural properties of the hydrogel, such as the pore size and thickness, and 2) the DEP conditions. These structural properties and DEP conditions can be easily changed by adjusting the composition of the hydrogel and the intensity of the applied voltage.

5. Conclusions

Our proposed SME sensor, combining the porous hydrogel and hDEP force, ensures high sensitivity and selectivity in Aβ analysis. Consequently, our sensor can quantify various disease-related proteins of known sizes with high sensitivity, providing high utility for the early diagnosis of various diseases besides AD. Although the size of albumin, the most abundant protein in the plasma, is only 69 kDa (approximately 3.8 nm) (Kiselev et al., 2001), the antifouling effect of the hydrogel was confirmed to be slightly insignificant, which can be sufficiently improved by more precisely controlling the pore size of the hydrogel. Therefore, in the following study, we plan to more precisely control the pore size of the hydrogel and study the cause for the enhancement of sensor sensitivity using the hDEP force. Ultimately, we plan to utilize our sensor that combines the passive filtration effect of hydrogel with the active filtration effect of DEP to perform plasma-based disease diagnosis with high accessibility, affordability and low invasiveness.

CRediT authorship contribution statement

Hye Jin Kim: Conceptualization, Methodology, Validation, Formal analysis, Investigation, Writing – original draft, Writing – review & editing, Visualization. **Woongsun Choi:** Conceptualization, Methodology, Validation, Formal analysis, Investigation, Writing – original draft, Writing – review & editing, Visualization. **Jin San Lee:** Data curation, Investigation, Validation, Writing – original draft, Writing – review & editing. **Jungkyu Choi:** Writing – review & editing, Supervision. **Nakwon Choi:** Conceptualization, Methodology, Writing – review & editing, Supervision. **Kyo Seon Hwang:** Conceptualization, Writing – review & editing, Supervision, Funding acquisition.

Declaration of competing interest

The authors declare that they have no known competing financial interest.

Acknowledgements

This work was supported by the National Research Foundation of Korea [grant numbers NRF-2021R1A2C2004760, NRF-2021R1C1C2004400, and NRF-2018M3C7A1056896] and the Korea Health Industry Development Institute [grant number HU21C0053].

Appendix A. Supplementary data

Supplementary data to this article can be found online at https://doi.org/10.1016/j.bios.2021.113668.

References

Abd Rahman, N., Ibrahim, F., Yafouz, B., 2017. Sensors (Basel) 17.
Ahmed, E.M., 2015. J. Adv. Res. 6, 105–121.
Alonso, R., Jimenez-Meneses, P., Garcia-Ruperez, J., Banuls, M.J., Maquieira, A., 2018. Chem. Commun. 54, 6144–6147.
Arevalo-Rodriguez, I., et al., 2013. Am. J. Alzheimers Dis. Other Demen. 28, 111–119.
Balasa, A.F., Chircov, C., Grumezescu, A.M., 2020. Biomedicines 8.
Buenger, D., Topuz, F., Groll, J., 2012. Prog. Polym. Sci. 37, 1678–1719.
Citron, M., 2002. Nat. Neurosci. 5 (Suppl. l), 1055–1057.
Dos Santos Picanco, L.C., et al., 2018. Curr. Med. Chem. 25, 3141–3159.
Ekblad, T., et al., 2008. Biomacromolecules 9, 2775–2783.
Fandos, N., et al., 2017. Alzheimer's & Dementia: diagnosis. Assessment & Disease Monitoring 8, 179–187.
Hansson, O., Lehmann, S., Otto, M., Zetterberg, H., Lewczuk, P., 2019. Alzheimer's Res. Ther. 11, 1–15.
Kausaite-Minkstimiene, A., Ramanaviciene, A., Kirlyte, J., Ramanavicius, A., 2010. Anal. Chem. 82, 6401–6408.
Khoury, R., Ghossoub, E., 2019. Biomarkers in Neuropsychiatry 1, 100005.
Kim, H.J., et al., 2016. Biosens. Bioelectron. 85, 977–985.
Kim, J., et al., 2018. PloS One 13, e0190451.
Kim, H.J., et al., 2019. Biosens. Bioelectron. 128, 166–175.
Kim, H.J., et al., 2020. Sensor. Actuator. B Chem. 302, 127190.
Kiselev, M.A., Gryzunov Iu, A., Dobretsov, G.E., Komarova, M.N., 2001. Biofizika 46, 423–427.
Le Goff, G.C., Srinivas, R.L., Hill, W.A., Doyle, P.S., 2015. Eur. Polym. J. 72, 386–412.
Lee, J.C., Kim, S.J., Hong, S., Kim, Y., 2019. Exp. Mol. Med. 51, 1–10.
Lee, H.J., Kim, J.Y., Roh, Y.H., Kim, S.M., Bong, K. W., 2019. Analyst 144, 6712–6720.
Leigh, B.L., et al., 2018. Langmuir 35, 1100–1110.
Lin, E.C., 2010. Mayo Clin. Proc. 85, 1142–1146.
Makaraviciute, A., Jackson, C.D., Millner, P.A., Ramanaviciene, A., 2016. J. Immunol. Methods 429, 50–56.
Mehta, P.D., et al., 2000. Arch. Neurol. 57, 100–105.
Murosaki, T., Ahmed, N., Ping Gong, J., 2011. Sci. Technol. Adv. Mater. 12, 064706.
Naahidi, S., et al., 2017. Biotechnol. Adv. 35, 530–544.
Ostuni, E., Chapman, R.G., Holmlin, R.E., Takayama, S., Whitesides, G.M., 2001. Langmuir 17, 5605–5620.
Pregibon, D.C., Doyle, P.S., 2009. Anal. Chem. 81, 4873–4881.
Saint-Aubert, L., et al., 2013. EJNMMI Res. 3, 43.
Sawayama, J., Takeuchi, S., 2021. Adv. Healthc. Mater. 10, 2001286.
Schneider, M.H., Tran, Y., Tabeling, P., 2011. Langmuir 27, 1232–1240.
Tokuda, T., et al., 2014. Biomed. Opt Express 5, 3859–3870.
Van Gerwen, P., et al., 1998. Sensor. Actuator. B Chem. 49, 73–80.
Wang, R., Li, Y., 2013. Biosens. Bioelectron. 42, 148–155.
Wong, W., 2020. Am. J. Manag. Care 26, S177–S183.